RSC Advances

ROYAL SOCIETY OF CHEMISTRY

www.rsc.org/advances

Cite this: DOI: 10.1039/c0xx00000x

www.rsc.org/xxxxxx

Paper

Sulfur/bamboo charcoal composites cathode for lithium–sulfur batteries

J. J. Cheng,[a,b] Y. Pan,*[a,b] J. A. Pan,[a,b] H. J. Song,[a,b] and Z. S. Ma*[a,b]

Received (in XXX, XXX) Xth XXXXXXXXX 20XX, Accepted Xth XXXXXXXXX 20XX
DOI: 10.1039/b000000x

Herein, sulfur/bamboo charcoal (S/BC) composites with sulfur content of 57.7 wt.% were prepared by melt–diffusion method as cathode materials for Li–S battery. An initial specific discharge capacity of 685 mAh g^{-1} and a reversible capacity of 414 mAh g^{-1} were obtained after 500 cycles at 0.5 C (1 C=1675 mA g^{-1}) rate, with only 0.079% capacity fade. Meanwhile, the S/BC cathode can deliver a stable discharge capacity at the current density from 0.1 C to 3 C. The improved cycle stability and rate capability of the S/BC composite cathode materials can be attributed to the well-connected, highly ordered porous structure of BC and the self-deposied passivation layer on Li anode.

Introduction

Lithium–sulfur (Li–S) batteries hold great potential for the next generation energy storage system to provide sufficient energy density at a lower cost.[1, 2] The elemental sulfur as the cathode active material can deliver a theoretical specific capacity of 1675 mAh g^{-1} and a theoretical specific energy of 2600 Wh kg^{-1} for the complete conversion to Li_2S. Additionally, sulfur possesses advantages of abundance in nature, low price and environmental friendliness.[3, 4] However, many problems hinder the practical applications of Li–S batteries. Among the serious issues is the high solubility of intermediate lithium polysulfides and the 'polysulfide shuttle' in the liquid electrolyte during charge and discharge resulting in poor cycling stability and low coulombic efficiency.[5, 6]

Various strategies have been reported to tackle the problem from the perspective of cathode, electrolyte, and anode, respectively. For the cathode, various porous carbon materials have been employed in cathode to trap polysulfides based on the high surface area and immobilization of sulfur within porous structures.[7-11] It is worth noting that the physical or chemical characteristics restricted by the synthesis process and the source of carbon, such as pore size distribution and mesoporous/microporous adsorption capability, play a particularly crucial role in the sulfur electrode[6, 12] and influence the electrochemical performance of the resultant composite cathode.[13, 14] For the electrolyte, the addition of polysulfides[15-18] or the increase of lithium salt concentration[19-21] in electrolyte have been demonstrated to block the polysulfide dissolution. For the anode, a passivation layer promoted by the additives on the Li anode surface can not only eliminate the polysulfide shuttle but also stabilize the interface of the Li anode.[22, 23]

It is worth emphasizing that the interaction and integration among the cathode, anode and electrolyte in the Li–S battery is obvious. For instance, the porous structure and high conductivity of the carbon matrix facilitates ion and electron transport and the dissolved polysulfides from the sulfur cathode can improve the concentration of electrolyte. As well, the dissolved polysulfides have been proved to play a significant role on the surface of Li anode and passivate the Li anode partially.[24, 25] Based on the above considerations, it can be speculated that employing an appropriate matrix for sulfur cathode which can facilitate ion and electron transport among sulfur and induce dissolved polysulfides to level the concentration gradient between the cathode and electrolyte and deposit a dense and integrated passivation layer on Li anode surface may be a strategy to enhance the cycling stability.

To test this hypothesis, here, the bamboo charoal (BC) as a matrix for sulfur cathode for Li–S batteries is reported. BC is of well-connected, highly ordered porous structure, high conductivity[26], outstanding adsorption property[27] and weak constraint to sulfur, some different from the frequently used microporous/mesoporous carbon, which is expected to facilitate ion and electron transport among sulfur and then induce lithium polysulfides to electrolyte and lead to a self-deposition of passivation layer to the surface of Li anode. Meanwhile, BC is biomass carbon with advantages of reproducibility, eco-friendly source, low cost and of flexibility for various modifications, complementing the cheap Li–S batteries.[28-31] The electrochemical performances of the sulfur/bamboo charcoal (S/BC) cathode were investigated systematically and a low long-term capacity fading rate and a stable rate capacity can be obtained even after 500 cycles. The results show that the strong pore structure of BC and the induced passivation layer on Li anode surface could contribute to the improved cycle stability and rate capability of the S/BC composite cathode materials.

Experimental

Sulfur/bamboo charcoal composite material synthesis

Sulfur/bamboo charcoal composite materials were synthesized via a melt–diffusion strategy. First, commercial bamboo charcoal (purity of >95 wt.%) was purified in ethanol using ultrasonic for 30 min and then dried at 60 °C for 12 h in vacuum. Then, in a

Cite this: DOI: 10.1039/c0xx00000x

www.rsc.org/xxxxxx

Paper

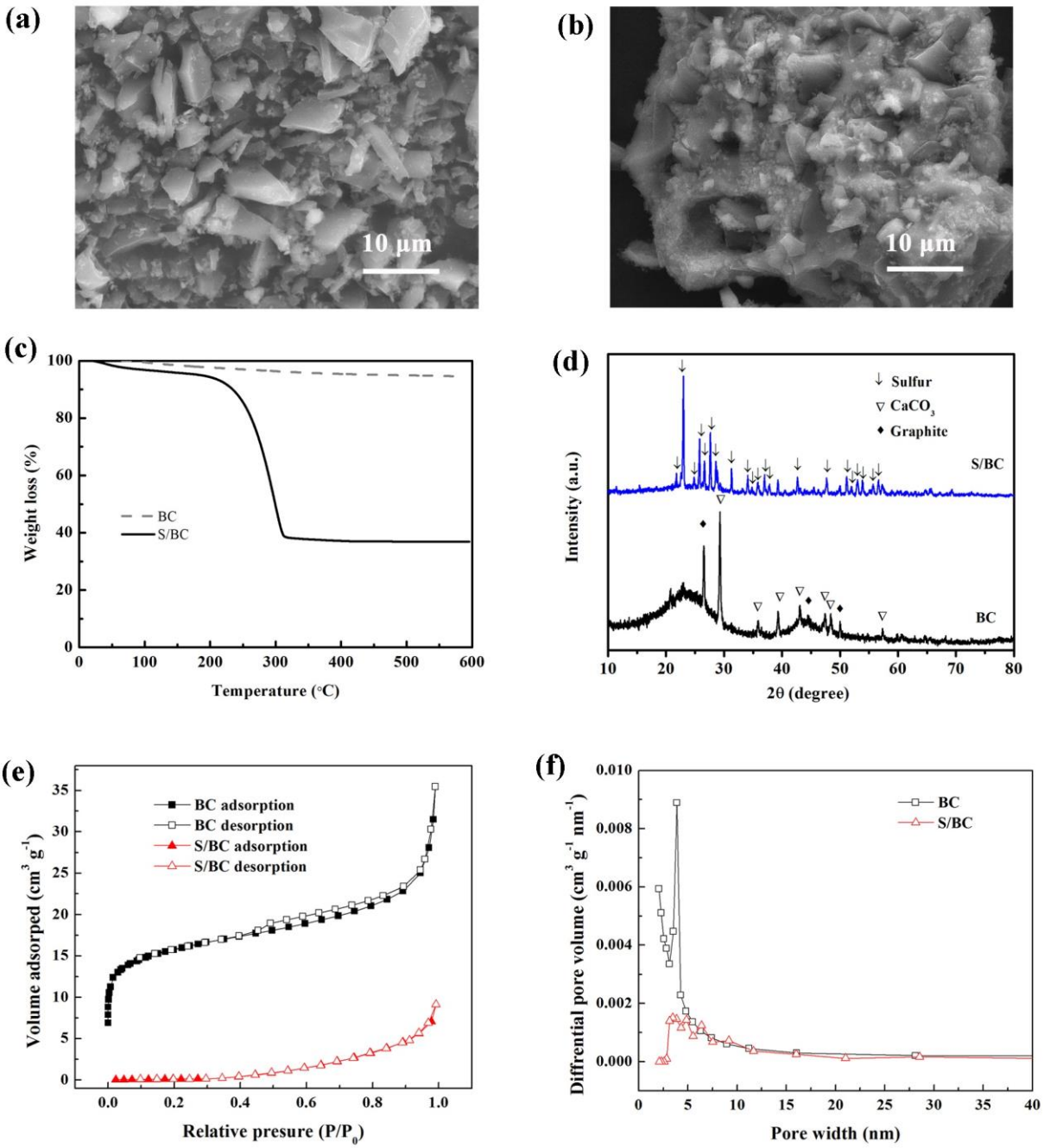

Fig. 1 SEM images of the (a) bamboo charcoal (BC) and (b) prepared sulfur/bamboo charcoal (S/BC) composites; (c) TGA curves of BC and S/BC; (d) XRD patterns of BC and S/BC; (e) N_2 adsorption–desorption isotherm curves and (f) BJH pore size distributions of the BC and S/BC.

typical synthesis, a weight ratio of 3 to 2 of sulfur and BC were homogeneously mixed and sintered at 100 °C for 4.5 h in vacuum to obtain S/BC composite materials. A control composite was prepared through the same strategy except for replacing BC with acetylene black.

XRD and SEM were used to characterize the microstructures and morphologies of BC, S/BC composite and cycled Li anode. Thermal gravimetric analysis (TGA) was conducted with a TGA

Cite this: DOI: 10.1039/c0xx00000x

www.rsc.org/xxxxxx

Paper

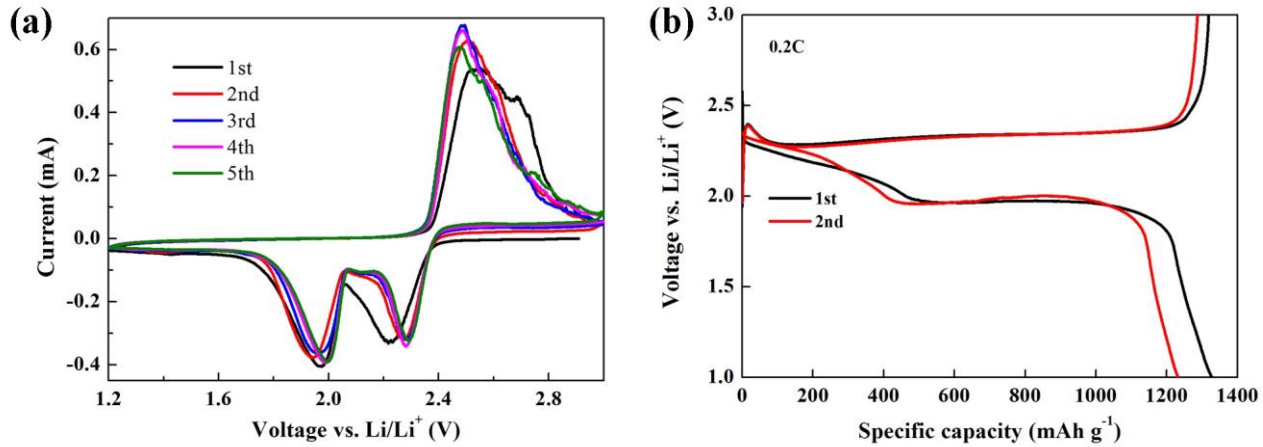

Fig. 2 (a) Cyclic voltammogram profiles of the S/BC cathode at a scan rate of 0.1 mV s^{-1}; (b) Galvanostatic charge/discharge profiles of the initial two cycles at the current density of 0.2 C (1 C=1675 mA g^{-1}).

Q50 thermo gravimetric analyzer in nitrogen at a scan rate of 10 °C/min from room temperature to 600 °C to determine the sulfur content of S/BC composites. N_2 sorption analysis was performed on a Beishide 3H-2000PS2 type analyzer at 77 K using nitrogen. The surface area was calculated using the BET method based on adsorption data with the partial pressure (P/P_0) ranging from 0.04 to 0.32 and the total pore volume was determined from the amount of nitrogen adsorbed at P/P_0 =0.99. The pore size distribution plot was derived from the desorption branch of the isotherm based on Barrett–Joyner–Halenda (BJH) model.

Electrochemical measurements

The cathode was prepared by mixing 70 wt.% S/BC, 20 wt.% acetylene black, and 10 wt.% polyvinylidene fluoride as binders in N-methylpyrrolidone, casted onto aluminum foils and then dried at 40 °C for 12 h in vacuum.

Electrochemical measurements of S/BC electrode were performed using Coin-type 2016 cells with lithium metal as the counter and reference electrode and a microporous membrane (Celgard 2400) as the separator. The electrolyte was 1 M lithium bis (tri-fluoromethanesulfonyl) imide (LiTFSI) dissolved in a 1:1 volume ratio mixture of 1, 3-dioxolane and Dimethoxy ethane. The cells were assembled in an argon-filled glove box.

All the electrochemical measurements were carried out at room temperature. Electrochemical charge/discharge and cycle performance, under the potential window 3.0 to 1.0 V (vs. Li/Li^+) at different current densities (1 C=1675 mA g^{-1}), were conducted using Battery Test System. The specific capacities were calculated on the mass of sulfur, and the composites loading was about 2–2.5 mg cm^{-2}. Cyclic voltammetry (CV) curves were measured by a CHI660D Electrochemical Workstation between 1.2 and 3.0 V at a scan rate of 0.1 mV s^{-1}. EIS was also measured by the CHI660D Electrochemical Workstation in a frequency range of 1 MHz to 0.1 Hz with an AC voltage amplitude of 5 mV at the open–circuit voltage.

Results and discussion

Figs. 1a and b display the SEM images of BC and S/BC composites, respectively, it can be seen that sulfur and BC particles have aggregated to form the S/BC cluster, with a particle size range from several tens of micron to hundreds micron, several times larger than that of BC. Sulfur is surrounded by BC in S/BC composites, other than being restricted within mesopores/micropores.

TGA curve of S/BC shows that the major weight loss occurs from about 200 to 400 °C due to the evaporation of sulfur along with a small weight loss from 50 to 200 °C belong to the volatile impurities of BC in Fig. 1c. The sulfur content is calculated based on the weight loss of the sulfur from room temperature to 600 °C. For the S/BC composite, the sulfur content is calculated to be 57.7 wt.%, being consistent with the design content.

As shown in the XRD patterns of BC and S/BC in Fig. 1d, the BC material is mainly amorphous carbon around 24° and 44° with some graphite near 27° and $CaCO_3$.[32, 33] The process of removing $CaCO_3$ with HCl is not done to shorten workflow and reduce costs. However, the XRD pattern of S/BC is completely different from the pure BC, which is similar to that of elemental sulfur. The sharp diffraction peaks indicate that sulfur is mainly in a crystalline state and surrounds the BC.[11, 34]

Along with the XRD pattern and SEM images, the surface area and pore size distribution were obtained to determine the dispersion and state of sulfur in S/BC composite. The nitrogen adsorption/desorption isotherms and the pore size distributions of BC and S/BC were shown in Fig. 1e and f, respectively. BC shows the type IV shape of the isotherm according the IUPAC, indicating the presence of mesopores.[8] The BC has a pore size of

Cite this: DOI: 10.1039/c0xx00000x

www.rsc.org/xxxxxx

Paper

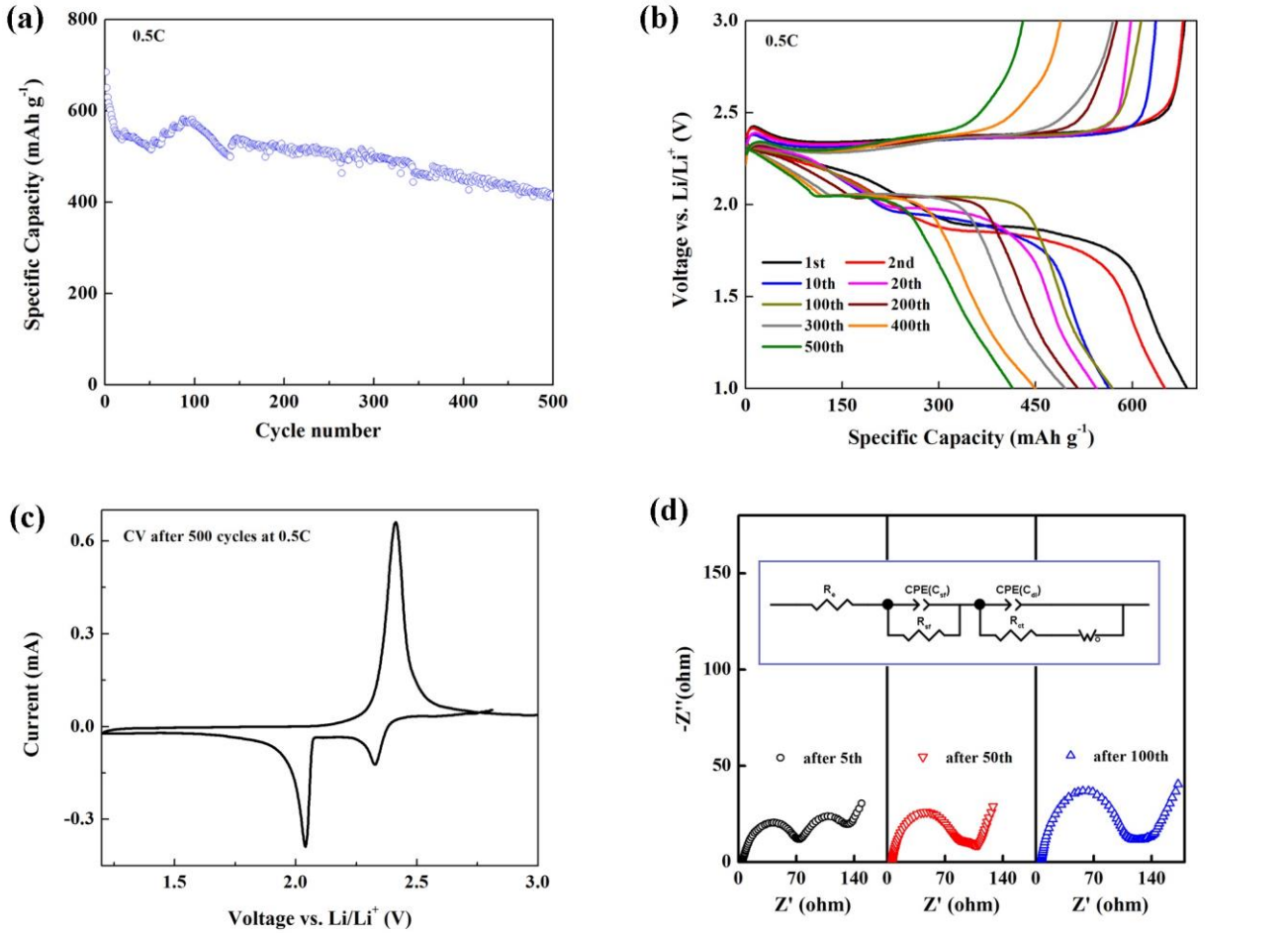

Fig. 3 (a) Cycling performance and (b) charge/discharge profiles of the S/BC cathode at 0.5 C over 500 cycles; (c) Cyclic voltammograms of the S/BC composite cathode after 500 cycles at a scan rate of 0.1 mV s^{-1}; (d) Electrochemical impedance spectroscopy plots of the S/BC cathodes after 5th, 50th and 500th cycle at 0.5 C rate (1 C=1675 mA g^{-1}), and insert shows the equivalent circuit of the system.

approximately 4 nm with a BET surface area of 57.8 m^2 g^{-1} and pore volume of 0.05 cm^3 g^{-1}. In contrast, S/BC has a surface area of 0.6 m^2 g^{-1} and pore volume of 0.01 cm^3 g^{-1}.[30, 35] About 13 wt.% of sulfur in S/BC composite can trap into the mesopores of BC theoretically and most sulfur covered on the surface of BC, which is corresponding to the SEM and XRD results.

The electrochemical reactions of S/BC composite as cathode for Li–S batteries were systematic investigated. Fig. 2a shows the CV curves of the S/BC composite cathode in the initial 5 cycles. In the cathodic scan process, two sharp reduction peaks at around 2.3 V and 2.0 V are observed, which are corresponding to the reduction of sulfur to long chain lithium polysulfides (Li_2S_n,4≤ n<8) and further reduction to Li_2S_2/Li_2S.[36, 37] In the subsequent anodic scan process, the oxidation peak at around 2.5 V can be ascribed to the oxidation of Li_2S_2/Li_2S to long chain lithium polysulfides.[38] Significantly, the reduction peaks at around 2.3 V and 2.0 V slightly shift to higher potentials and the oxidation peak at around 2.5 V shifts to lower potential, exhibiting electrochemical reversibility and stability. The initial two charge/discharge profiles of S/BC composite cathode at the current density of 0.2 C (1 C=1675 mA g^{-1}) are shown in Fig. 2b. It can be seen that the discharge and charge voltage plateaus resemble the reduction and oxidation peaks appearing in the CV curves. The S/BC composite cathode delivered an initial specific discharge capacity of 1325 mAh g^{-1} and a reversible charge capacity of 1319 mAh g^{-1} at a current rate of 0.2 C. A specific discharge capacity of 1232 mAh g^{-1} is obtained in the second cycle, showing an irreversible capacity of 93 mAh g^{-1} compared with the initial capacity.

The cycling performance of S/BC composite cathodes at a current rate of 0.5 C are shown in Fig. 3a. The initial specific discharge capacity and the reversible charge capacity are 685

Cite this: DOI: 10.1039/c0xx00000x

www.rsc.org/xxxxxx

Paper

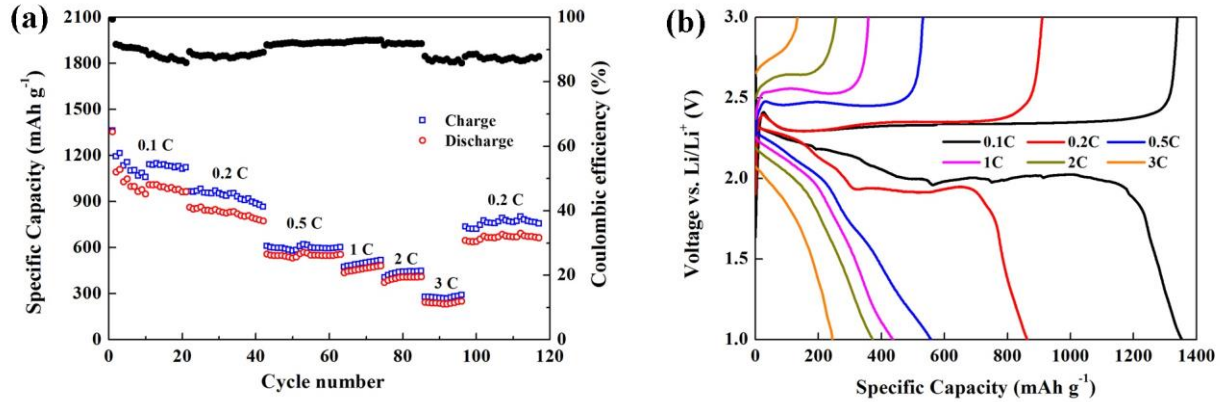

Fig. 4 (a) Rate capability and (b) the typical charge/discharge profiles of the S/BC cathode at the current density from 0.1C to 3C and recovered to 0.2C rate (1C=1675 mA g^{-1}).

mAh g^{-1} and 681 mAh g^{-1}, respectively, exhibiting a very small irreversible capacity. Even after a long cycling of 500 cycles, a discharge capacity still reaches 414 mAh g^{-1} corresponding to an ultra-low fading rate of 0.079% per cycle.[39] The cycle performance is superior relative to sulfur–acetylene black composites,[35] showing the advantage of S/BC. Fig. 3b shows the selected charge/discharge profiles of S/BC composite cathodes at 0.5 C. It can be seen that the plateaus in all the charge/discharge profiles during cycle agree well with the reduction and oxidation peaks observed in the CV curves in Fig. 2a. In the discharge profiles, the lower plateaus rise gradually with the cycle number, being consistent with the shift of reduction peaks in the CV curves. After 500 cycles, the reduction and oxidation plateaus in the charge/discharge profiles still remain clear, indicating a high electrochemical stability. The CV curve was measured to identify the reduction and oxidation after 500 cycles at the current rate of 0.5 C (Fig. 3c). The sharp cathode peaks at 2.33 V and 2.04 V and the anodic peak at 2.41 V are corresponding to the discharge plateaus and the charge plateau in the 500th cycle. In all, the S/BC composite cathodes display an excellent electrochemical reversibility and a long cycle life.

To study the degradation of the cell, EIS was measured on the completely charged state of the cell after 5th, 50th and 100th cycles at 0.5 C, as shown in Fig. 3d. The impedance spectra exhibit two depressed semicircle and an inclined line in the high-, middle- and low-frequency region, which are attributed to the charge transfer resistance at the electrode/electrolyte interface, the resistance of the solid-electrolyte-interface (SEI) layer and the Warburg impedance due to the polysulfides diffusion process, respectively.[40] A corresponding equivalent circuit (inset of Fig. 3d) is proposed to describe the EIS results. R_e represents the impedance contributed by the resistance of the electrolyte, R_{sf} and C_{sf} are the resistance and capacitance of the SEI layer. R_{ct} and C_{dl} are the resistance and capacitance of the charge transfer resistance at the electrode/electrolyte interface, and W_o represents the Warburg impedance.[41, 42] In Fig. 3d, it shows that the value of R_e (4.68, 6.32, and 5.67 Ω after 5th, 50th and 100th cycle) change slightly, R_{ct} (73.4, 84.3, and 113 Ω after 5th, 50th and 100th cycle) increases and R_{sf} decreases gradually during the 100 cycles. Combining EIS results with the cycle performance in Fig. 3a, it could be deduced that irreversible Li_2S deposited on the surface of S/BC cathode slightly caused the increase of R_{ct} and the capacity degradation during the initial 50 cycles. The reversibility of the cell becomes well from 50 to 100 cycles and the discharge capacity remains stable even to 500 cycles.

The rate performance of S/BC composite cathode cycled at current rates ranges from 0.1, 0.2, 0.5, 1, 2 to 3 C and then back to 0.2 C is shown in Fig. 4. The initial capacities are 1354, 966, 558, 481 and 407 mAh g^{-1} at 0.1, 0.2, 0.5, 1 and 2 C, respectively. A specific discharge capacity of 250 mAh g^{-1} with a coulombic efficiency more than 85 % is obtained at 3 C, and the capacity recovers to 646 mAh g^{-1} when the rate reduces back to 0.2 C, indicating a good rate capacity compared with the sulfur/activated-conductive carbon black composites cathode.[43] The corresponding charge/discharge profiles at different rates are shown in Fig. 4b. All the charge/discharge profiles consisting of two reduction plateaus and an oxidation plateaus agree well with the redox peaks in CV scans (Fig. 3a). And electrochemical polarization at higher current rates is obvious, which may be due to that sulfur is on the surface of BC.

To disclose the reason for the long cycle life and good rate capacity of S/BC composite, a control S/acetylene black composite was investigated. Actually, as shown in Fig. 5a, the control cell after 60 cycles decreased to only 178 mAh g^{-1}, showing only 10.6% utilization of the sulfur, which is far from practical application and also lost the discharge/charge plateaus. While the S/BC composite displayed an initial specific discharge capacity of 876 mAh g^{-1} and retained at 612 mAh g^{-1} after 60 cycles. Based on the interaction and integration of Li–S battery in mind, the surface morphology and structure of the cycled Li

Cite this: DOI: 10.1039/c0xx00000x

www.rsc.org/xxxxxx

Paper

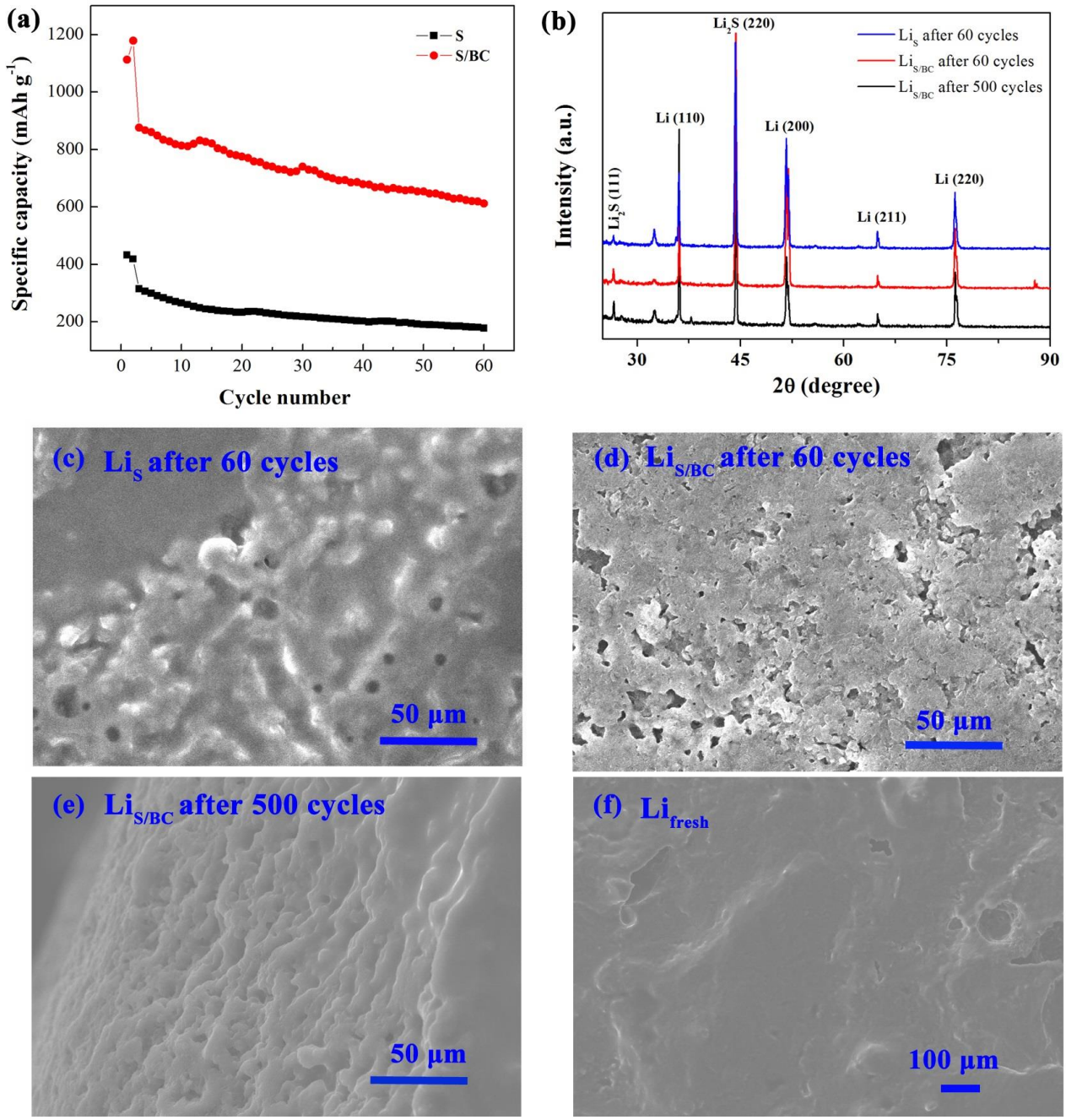

Fig. 5 (a) Cycle performance of S/BC and S/acetylene black; (b) XRD pattern of the cycled Li anode; SEM images of the cycled Li anode from (c) the S/acetylene black and (d) S/BC composite cells after 60 cycles, (d) from S/BC composite cells after 500 cycles; (e) SEM image of the fresh Li metal.

anode (Li_S) from the control cell and anode (Li_{BC}) from the S/CB composite cell cycled 60 cylces were investigated by XRD and SEM. A layer of passivation was observed on the cycled Li_{BC} surface (Fig. 5d), while there were only corrosive lines on the Li_S (Fig. 5c). The layer was indexed to be Li_2S by the XRD pattern (Fig. 5b). The phenomena may be due to that the S/BC could activate more sulfur to reduction and promise larger contact area with the electrolyte.

Further, the cycled Li anode from the S/BC after 500 cycles was also studied shown in Fig. 5e. There is a more stable dense and roughness layer on the surface of the cycled Li, which seems to be an evolution with cycling in contrast to the cycled Li anode

after 60 cycles and absolutely different with that on the fresh Li metal (Fig. 5f). The layer was indexed to be Li_2S by the XRD pattern (Fig. 5b). This passivation layer can help impede the penetration of polysulfides and provide the ion pathway, leading to a long-term cycle stability and good rate performance.[23]

Genenally speaking, the good stability of Li–S batteries is resulted from the immobilization of polysulfides at the cathode region, the blocked polysulfide dissolution in the electrolyte or the protection of Li anode surface.[23, 39, 44] For the bamboo charcoal/sulfur composites, the BC matrix possesses a small specific surface area, poor microporous or mesoporous structure. So BC plays a key role to enhance the charge and ion transport and is limited for immobilizing the active material and polysulfides.[6] Combing the above results, it could assume that the the well-connected and ordered porous BC could activate large amount of sulfur into reduction at the same time and then induce a certain amount of polysulfides into electrolyte due to the concentration gradient at the electrode/electrolyte interface. The reduction of polysulfides on the Li metal could react with the Li metal and promote a solid electrolyte interphase layer on the surface of Li anode.

Conclusions

In summary, a renewable, low cost and scalable activated carbon obtained from bamboo has been successfully used as the host of sulfur to design the S/BC composites cathode for stable Li–S battery. An initial specific discharge capacity of 685 along with a fading rate of 0.079% (0.5 C, 500 cycles) is obtained for the S/BC composite materials. The stability of S/BC composite cathode is attributed to the special pore structure of the bamboo charcoal and the stable solid electrolyte interphase layer self-deposited on Li anode. The detailed process for the formation of the Li protect layer will be studied in the future. The overall stability of the S/BC composite cathode accompanied by a stable anode is good. Besides, with appealing performance at higher charge/discharge rates the S/BC composite is of significant promise for high energy/power density rechargeable batteries.

Acknowledgements

We gratefully acknowledge financial support from the National Natural Science Foundation of China (Nos. 11372267 and 11102176), the Emerging Strategic Industries of Hunan Province (2012GK4075), the Science and Technology Program of Hunan Province (2013GK3163) and the Graduate Innovation Program of Hunan Province (CX2013B258)

Notes and references

[a] *National–Provincial Laboratory of Special Function Thin Film Materials, Xiangtan University, Xiangtan 411105, Hunan, China. Fax: +86-731-58293577; Tel: +86-731-58293577; E-mail: ypan@xtu.edu.cn, zsma@xtu.edu.cn*

[b] *School of Materials Science and Engineering, Xiangtan University, Xiangtan 411105, Hunan, China.*

1. M. Armand and J.-M. Tarascon, *Nature*, 2008, **451**, 652-657.
2. P. G. Bruce, S. A. Freunberger, L. J. Hardwick and J.-M. Tarascon, *Nat. Mater.*, 2012, **11**, 19-29.
3. X. Ji and L. F. Nazar, *J. Mater. Chem.*, 2010, **20**, 9821-9826.
4. L. F. Nazar, M. Cuisinier and Q. Pang, *MRS Bull.*, 2014, **39**, 436-442.
5. Y. V. Mikhaylik and J. R. Akridge, *J. Electrochem. Soc.*, 2004, **151**, A1969-A1976.
6. A. Manthiram, Y. Fu, S. H. Chung, C. Zu and Y. S. Su, *Chem. Rev.*, 2014.
7. H. B. Wu, S. Wei, L. Zhang, R. Xu, H. H. Hng and X. W. Lou, *Chemistry*, 2013, **19**, 10804-10808.
8. J. Schuster, G. He, B. Mandlmeier, T. Yim, K. T. Lee, T. Bein and L. F. Nazar, *Angew. Chem. Int. Ed.*, 2012, **51**, 3591-3595.
9. S. Thieme, J. Brückner, I. Bauer, M. Oschatz, L. Borchardt, H. Althues and S. Kaskel, *J. Mater. Chem. A*, 2013, **1**, 9225.
10. N. Jayaprakash, J. Shen, S. S. Moganty, A. Corona and L. A. Archer, *Angew. Chem. Int. Ed.*, 2011, **50**, 5904-5908.
11. L. Ji, M. Rao, S. Aloni, L. Wang, E. J. Cairns and Y. Zhang, *Energy Environ. Sci.*, 2011, **4**, 5053-5059.
12. X. Li, Y. Cao, W. Qi, L. V. Saraf, J. Xiao, Z. Nie, J. Mietek, J.-G. Zhang, B. Schwenzer and J. Liu, *J. Mater. Chem.*, 2011, **21**, 16603.
13. N. Ding, S. W. Chien, T. S. A. Hor, Z. Liu and Y. Zong, *J. Power Sources*, 2014, **269**, 111-116.
14. C. Barchasz, J.-C. Leprêtre, F. Alloin and S. Patoux, *J. Power Sources*, 2012, **199**, 322-330.
15. S. Chen, F. Dai, M. L. Gordin and D. Wang, *RSC Adv.*, 2013, **3**, 3540.
16. D. J. Lee, M. Agostini, J. W. Park, Y. K. Sun, J. Hassoun and B. Scrosati, *ChemSusChem*, 2013, **6**, 2245-2248.
17. N. Li, Z. Weng, Y. Wang, F. Li, H.-M. Cheng and H. Zhou, *Energy Environ. Sci.*, 2014, **7**, 3307-3312.
18. R. Xu, I. Belharouak, J. C. M. Li, X. Zhang, I. Bloom and J. Bareño, *Adv. Energy Mater.*, 2013, **3**, 833-838.
19. L. Suo, Y. S. Hu, H. Li, M. Armand and L. Chen, *Nat. Commun.*, 2013, **4**, 1481.
20. E. S. Shin, K. Kim, S. H. Oh and W. I. Cho, *Chem. Commun.*, 2013, **49**, 2004-2006.
21. Y. Zhang, S. Liu, G. Li, G. Li and X. Gao, *J. Mater. Chem. A*, 2014, **2**, 4652-4659.
22. F. Wu, J. Qian, R. Chen, J. Lu, L. Li, H. Wu, J. Chen, T. Zhao, Y. Ye and K. Amine, *ACS Appl. Mater. Interfaces*, 2014, **6** 15542-15549.
23. Z. Lin, Z. Liu, W. Fu, N. J. Dudney and C. Liang, *Adv. Funct. Mater.*, 2013, **23**, 1064-1069.
24. S. Xiong, K. Xie, Y. Diao and X. Hong, *J. Power Sources*, 2013, **236**, 181-187.
25. R. Demir-Cakan, M. Morcrette, Gangulibabu, A. Gueguen, R. Dedryvere and J.-M. Tarascon, *Energy Environ. Sci.*, 2013, **6**, 176-182.
26. Q. W. Jiang, G. R. Li, F. Wang and X. P. Gao, *Electrochem. Commun.*, 2010, **12**, 924-927.
27. C. Moreno-Castilla, *Carbon*, 2004, **42**, 83-94.
28. M. Depardieu, R. Janot, C. Sanchez, A. Bentaleb, C. Gervais, M. Birot, R. Demir-Cakan, R. Backov and M. Morcrette, *RSC Adv.*, 2014, **4**, 23971-23976.
29. R. Elazari, G. Salitra, A. Garsuch, A. Panchenko and D. Aurbach, *Adv. Mater.*, 2011, **23**, 5641-5644.
30. H. S. Ryu, J. W. Park, J. Park, J.-P. Ahn, K.-W. Kim, J.-H. Ahn, T.-H. Nam, G. Wang and H.-J. Ahn, *J. Mater. Chem. A*, 2013, **1**, 1573.
31. S. Zhao, C. Li, W. Wang, H. Zhang, M. Gao, X. Xiong, A. Wang, K. Yuan, Y. Huang and F. Wang, *J. Mater. Chem. A*, 2013, **1**, 3334.
32. C. Jia-jia, J. Xin, S. Qiu-jie, W. Chong, Z. Qian, Z. Ming-sen and D. Quan-feng, *Electrochim. Acta*, 2010, **55**, 8062-8066.
33. Y. Cao, X. Li, I. A. Aksay, J. Lemmon, Z. Nie, Z. Yang and J. Liu, *Phys. Chem. Chem. Phys.*, 2011, **13**, 7660-7665.
34. J. Kim, D.-J. Lee, H.-G. Jung, Y.-K. Sun, J. Hassoun and B. Scrosati, *Adv. Funct. Mater.*, 2013, **23**, 1076-1080.
35. B. Zhang, C. Lai, Z. Zhou and X. P. Gao, *Electrochim. Acta*, 2009, **54**, 3708-3713.
36. A. G. H. Yamin, J. Penciner, Y. Sternberg, and E. Peled, *J. EIectrochem. Soc.*, 1988, **135**, 4.
37. S.-E. Cheon, K.-S. Ko, J.-H. Cho, S.-W. Kim, E.-Y. Chin and H.-T. Kim, *J. Electrochem. Soc.*, 2003, **150**, A796.
38. J. Akridge, *Solid State Ionics*, 2004, **175**, 243-245.
39. C. Huang, J. Xiao, Y. Shao, J. Zheng, W. D. Bennett, D. Lu, S. V. Laxmikant, M. Engelhard, L. Ji, J. Zhang, X. Li, G. L. Graff and J. Liu, *Nat. Commun.*, 2014, **5**, 3015.

40. L. Yuan, X. Qiu, L. Chen and W. Zhu, *J. Power Sources*, 2009, **189**, 127-132.
41. V. S. Kolosnitsyn, E. V. Kuzmina, E. V. Karaseva and S. E. Mochalov, *J. Power Sources*, 2011, **196**, 1478-1482.
42. N. A. Cañas, K. Hirose, B. Pascucci, N. Wagner, K. A. Friedrich and R. Hiesgen, *Electrochim. Acta*, 2013, **97**, 42-51.
43. G. C. Li, J. J. Hu, G. R. Li, S. H. Ye and X. P. Gao, *J. Power Sources*, 2013, **240**, 598-605.
44. S. S. Zhang and J. A. Read, *J. Power Sources*, 2012, **200**, 77-82.